Motion planning for obstacle avoidance in overhead cranes via artificial potential fields and model predictive control

Trong Nghia Phan[1], **Tien Dung Nguyen**[2], **Tung Lam Nguyen**[2] **and Quang Hieu Ngo**[1,*]

[1]*College of Engineering, Can Tho University*
[2]*School of Electrical and Electronic Engineering, Hanoi University of Science and Technology*
[*]*Corresponding author E-mail: nqhieu@ctu.edu.vn*
DOI: https://doi.org/10.64032/mca.v30i1.380

Abstract

This paper proposes a novel trajectory tracking and obstacle avoidance control method for crane systems in industrial environments. First, the reference motion trajectory of the trolley carrying the load, along with the time-varying cable length, is designed using a model predictive controller (MPC). A key contribution of this study is the application of the artificial potential field (APF)-based obstacle avoidance method to crane systems for the first time. Subsequently, a sliding mode controller (SMC) is developed to track the designed reference trajectory. The global stability and state convergence of the closed-loop system are rigorously proven using Lyapunov stability theory. Finally, simulation results on MATLAB/Simulink demonstrate the effectiveness of the proposed method.

Keywords: *Artificial potential field; Model predictive control; Obstacle avoidance; Overhead crane; Trajectory tracking control.*

Symbols

Symbols	Units	Description
m	kg	Load mass
m_r	kg	Trolley mass
g	ms^{-2}	Gravitational acceleration
x	m	Trolley position
l	m	Hoisting cable length
θ	rad	Load swing angle
u_1	N	Driving force applied to the trolley
u_2	N	Force for hoisting/lowering the load cable
x_l	m	Position of the trolley along the OX axis
z_l	m	Position of the load along the OZ axis
$\dot{x}$	ms^{-1}	Trolley velocity
$\dot{l}$	ms^{-1}	Cable hoisting/lowering velocity
$\dot{\theta}$	$rads^{-1}$	Swing angular velocity of the load
$\ddot{x}$	ms^{-2}	Trolley acceleration
$\ddot{l}$	ms^{-2}	Cable hoisting/lowering acceleration
$\ddot{\theta}$	$rads^{-2}$	Swing angular acceleration of the load

1. Introduction

Industrial cranes play a crucial role in transporting and handling goods at ports as well as in factories. This process requires smooth coordination between the trolley motion and the hoisting mechanism, ensuring both transport efficiency and swing suppression. The motions need to be performed simultaneously to shorten the travel time. However, when the system operates at high speed, the travel time is reduced but the swing amplitude of the load increases, posing risks to the cargo and surrounding structures [1], [2]. Conversely, when operating at low speed, the swing is reduced but the system productivity is limited. Therefore, designing a time-optimal motion trajectory for crane systems, while ensuring state constraints, is an important problem that needs to be addressed.

Over the past decades, the problems of anti-swing control and time-optimal motion planning for crane systems have attracted extensive research attention. To design a controller for a crane system, it is first necessary to establish its dynamic model. In the current industrial environment, the 2D crane model is widely applied, with three degrees of freedom (3DoF), including the trolley position, the cable length, and the load swing angle [3]. The control signals of the 2D crane system consist of the driving force applied to the trolley and the torque used to adjust the cable length; therefore, this system is considered an underactuated model. One of the earliest control approaches for this model is the input shaping method [4], which reduces the swing amplitude of the load by adjusting input pulses to avoid exciting the natural frequency of the system.

In parallel, another research direction has focused on optimal trajectory planning to shorten transport time and save energy. A time-optimal control model with velocity and acceleration constraints was introduced in [5], and later extended to the container crane problem with specific actuator characteristics [6]. The flatness property of the crane model was exploited in [7], allowing trajectory construction directly from flat outputs, thereby reducing computational burden and enhancing feasibility in practical implementation. Recently, with the rapid advancement of technology, the computational capacity of industrial computers has improved significantly, making model predictive control (MPC) a highly promising solution for crane control. MPC is capable of handling multi-input multi-output (MIMO) systems and directly incorporating constraints,

Received: 10 October 2025; Revised: 3 February 2026; Accepted: 11 February 2026.

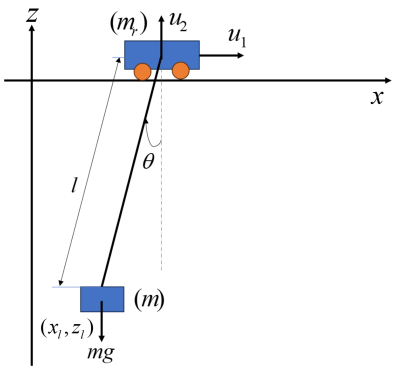

Figure 1: 2D crane model

thus ensuring accurate trajectory tracking while reducing load swing [8]. In summary, it can be observed that classical methods, although effective in reducing load oscillations, often neglect practical operational constraints. Traditional trajectory optimization solutions frequently encounter difficulties in real-time computation, whereas MPC handles constraints effectively but requires high computational cost. Recently developed integrated strategies, while promising, still demand further investigation to adapt to complex environments with obstacles. In [9], the authors introduced an MPC-based trajectory tracking control method for cranes, where obstacles are enclosed by ellipses. The MPC is then designed to optimize a cost function representing the motion time and the distance between the load and the ellipses. However, a limitation of this method is that the distance between the load and the ellipses is calculated using complex approximate formulas, which require significant computational resources. Chen and colleagues proposed designing the motion trajectory based on the flatness of the crane model [10]. The trajectories of the trolley and the hoisting cable are represented by high-order polynomials, with the polynomial order selected according to the number of states to be constrained and the corresponding number of obstacles. Recently, in [11], linearized intermediate signals were designed to simplify the crane model from nonlinear to linear, allowing trajectory design using time-based polynomials. Overall, the strength of the above methods lies in ensuring state constraints and obstacle avoidance for the crane. However, the polynomial order chosen for the reference trajectory must be fixed for different working conditions (number of obstacles, number of crane states to be constrained), resulting in low flexibility.

Based on the above analysis, this paper proposes an integrated control solution in which the reference trajectory of the trolley and the hoisting cable is optimized through a combination of MPC and the artificial potential field (APF), followed by trajectory tracking using a sliding mode controller (SMC). To the authors' knowledge, this is the first study to apply APF to the obstacle-avoidance trajectory planning problem of crane systems. In this approach, potential fields, including attractive and repulsive potentials, are constructed based on the interactions among the load, obstacles, and the target, and are then optimized within the MPC framework. Compared to trajectory design methods based on geometric constraints or complex polynomials, APF offers the advantages of a lightweight structure while expanding the feasible solution space, helping MPC avoid infeasibility issues. Furthermore, constraints on the load swing angle and the trolley's movement velocity are integrated into the proposed model to ensure feasibility and safety during operation. The main contributions of the paper can be summarized as follows:

1. APF Method: The paper applies the artificial potential field to describe the relationships among the load, obstacles, and the target within the crane's operating environment, where obstacles are enclosed by circles, simplifying the distance calculations. At the same time, the value of the total potential function can be adjusted through gain parameters, providing flexibility for the user to prioritize either obstacle avoidance or rapid achievement of the target.
2. Trajectory Optimization via MPC: The total potential field, operation time, and the system's physical constraints are integrated into the model predictive control framework, allowing the optimization of the motion trajectory while ensuring compliance with the crane's kinematic constraints.

The remainder of this paper is organized as follows: Section 2 presents the motion planning for obstacle avoidance of the crane; Section 3 introduces the trajectory tracking controller; Section 4 provides the simulation results for validation; and finally, Section 5 concludes the paper.

2. Motion planning for obstacle avoidance

In this section, the reference trajectory of the trolley and the cable length are determined by the MPC through the APF optimization process.

2.1 Modeling for motion planning

Consider the 2D crane model illustrated in Figure 1. The model parameters and the coordinates of the physical structures of the crane are defined in detail in the List of symbols.

The dynamics of the 2D crane system are described according to [12]:

$$\begin{aligned} u_1 &= (m_r+m)\ddot{x}+m\begin{pmatrix}\ddot{l}\sin\theta+l\ddot{\theta}\cos\theta\\ +l\dot{\theta}^2\sin\theta+2\dot{l}\dot{\theta}\cos\theta\end{pmatrix}\\ u_2 &= m\ddot{l}+m\ddot{x}\sin\theta-ml\dot{\theta}^2+mg\cos\theta\\ 0 &= ml^2\ddot{\theta}+ml\ddot{x}\cos\theta+2ml\dot{l}\dot{\theta}+mgl\sin\theta \end{aligned} \tag{1}$$

By transforming expression (1), the swing angular acceleration $\ddot{\theta}$ is obtained as follows:

$$\ddot{\theta}=-\frac{1}{l}\left(\ddot{x}\cos\theta+2\dot{l}\ \dot{\theta}+g\sin\theta\right) \tag{2}$$

The position of the load is determined as follows [12]:

$$\begin{aligned} x_l &= x+l\sin\theta\\ z_l &= -l\cos\theta \end{aligned} \tag{3}$$

The vertical acceleration of the load obtained from expression (3) is as follows:

$$\ddot{z}_l=-\ddot{l}\cos\theta+2\dot{l}\sin\theta\dot{\theta}+l\cos\theta\dot{\theta}^2-l\sin\theta\ddot{\theta} \tag{4}$$

Remark 1. *In the practical crane control problem, it is essential to ensure that the load is delivered to the correct position (through the trolley position and the cable length), avoids collisions with obstacles, and maintains the load swing angle as small as possible. Expression (2) shows that variations in the load swing angle depend on the trolley position and the cable*

length. Therefore, selecting appropriate reference values for these two states will help minimize the load swing angle.

From the above analysis, in cases where the obstacle positions are known in advance, designing reference trajectories for the trolley and the hoisting cable before operating the crane will be more effective than relying solely on conventional trajectory tracking combined with anti-sway control [13]. In this way, the load swing angle can be kept small when the trolley and cable follow the predefined trajectory, meaning that the controller only needs to focus on the trajectory tracking performance of the trolley and the cable while the anti-sway component can be neglected.

2.2 Design of artificial potential fields

As analyzed in Remark 1, this section presents a method for designing the motion trajectory of the crane, specifically constructing the reference signals for the trolley position and the hoisting cable length. Let $\boldsymbol{\eta} = \left[x, l, \theta, \dot{x}, \dot{l}, \dot{\theta}\right]^\top$, and $\boldsymbol{u} = \left[\ddot{x}, \ddot{l}\right]^\top$, the derivative of $\boldsymbol{\eta}$ obtained from expressions (1) and (2) is as follows:

$$\begin{aligned}\dot{\boldsymbol{\eta}} &= f(\boldsymbol{\eta}, \boldsymbol{u}) \\ &= \begin{bmatrix} \boldsymbol{\eta}(4) \\ \boldsymbol{\eta}(5) \\ \boldsymbol{\eta}(6) \\ \boldsymbol{u}(1) \\ \boldsymbol{u}(2) \\ -\frac{1}{l}\left(\boldsymbol{u}(1)\cos\boldsymbol{\eta}(3) + 2\boldsymbol{\eta}(4)\ \boldsymbol{\eta}(6) + g\sin\boldsymbol{\eta}(3)\right) \end{bmatrix}\end{aligned} \tag{5}$$

Remark 2. *Model (5) describes the dependence of the trolley position, the cable length, the load swing angle, and their corresponding velocities on the trolley acceleration and the acceleration of cable-length variation. This indicates that the crane states can be completely predicted before these accelerations are applied. Combined with the APF method, which is prominent in obstacle-avoidance control, the paper proposes using the MPC approach to design the crane motion trajectory, in which APF is integrated to ensure obstacle avoidance.*

2.2.1 Attractive potential field

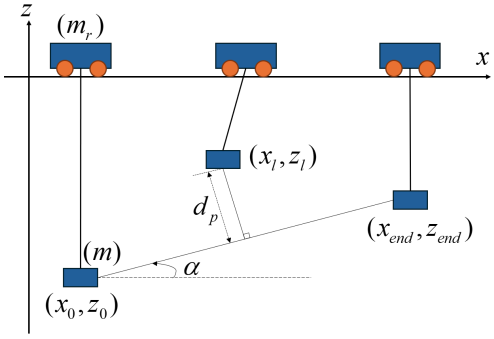

Figure 2: Virtual reference trajectory for the load m

Most of the previously introduced APF algorithms design the attractive potential field based on the distance between the vehicle and the target [14]. However, a noticeable limitation of this approach is that when the target is located far from the initial position of the load, the attractive potential field takes a very large value right from the beginning. As a result, the influence of the attractive component in the overall potential field becomes dominant, causing the designed trajectory to prioritize quickly reaching the target while paying less attention to obstacle avoidance.

In this paper, we construct a virtual reference trajectory for the load, determined based on the starting position and the required destination, as illustrated in Figure 2. The attractive potential for the reference path is designed as follows:

$$F_p = A_p d_p^2 \tag{6}$$

where d_p is the shortest distance from the load to the reference path, and d_p can be described as follows:

$$\begin{aligned} d_p &= (z_l - z_0)\cos\alpha - (x_l - x_0)\sin\alpha \\ \alpha &= \arctan\left(\frac{z_{\text{end}} - z_0}{x_{\text{end}} - x_0}\right) \end{aligned} \tag{7}$$

where α is the inclination angle of the reference path, and x_0, z_0 and x_{end}, z_{end} are the coordinates of the load's starting point and the required destination, respectively.

With the design of the attractive field in (6), F_p increases when the load deviates from the reference trajectory. This means that the load will tend to follow the reference trajectory and will certainly reach the destination if F_p is optimized to its minimum value.

2.2.2 Repulsive potential field

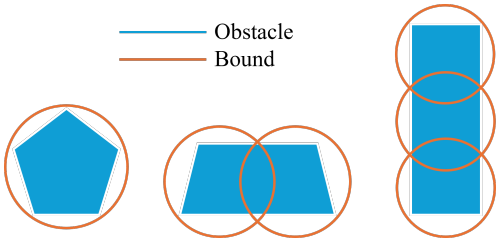

Figure 3: Different obstacles along with their corresponding envelopes

Similar to the design of the attractive potential field, the repulsive potential field is constructed based on the distance between the load and the obstacles. However, it should be noted that the shape of obstacles is often not well defined, making it difficult to calculate the exact shortest distance between the load and the obstacles. To address this, we use circles that cover the entire obstacles and then take the distance from the load to these circles as the basis for designing the repulsive potential. Some examples of obstacle shapes along with the corresponding selection of covering circles are illustrated in Figure 3.

When an obstacle is covered by n circles with radius r, the repulsive potential function is designed as follows:

$$\begin{aligned} F_{ob} &= \sum_{i=1}^{n} A_{ob} \exp\left(-\frac{d_{i,ob}^2}{2\sigma^2}\right) \\ d_{i,ob} &= \sqrt{(x_l - x_i)^2 + (z_l - z_i)^2} - r \end{aligned} \tag{8}$$

where x_i, z_i are the coordinates of the center of the i-th circle, and σ is the radius of the safety region around the obstacle.

It can be seen that with the design of F_{ob} in (8), the repulsive potential increases rapidly as the load approaches the region within a distance σ from the circle envelopes, and reaches its maximum value when the load collides with these envelopes. Therefore, by optimizing F_{ob} to its minimum value, the load is ensured not to collide with the envelopes, thereby avoiding the corresponding obstacle.

2.3 Motion planning design using MPC

To discretize the system while maintaining computational accuracy, the paper applies the fourth-order Runge-Kutta (RK4) method with a sampling time Δt. From (5), the discrete-time dynamics of the crane are established as $\boldsymbol{\eta}(j+1) = f(\boldsymbol{\eta}(j), \boldsymbol{u}(j))$.

The objective of the MPC is to find the solution $\boldsymbol{u}$ that minimizes the cost function. To ensure obstacle avoidance and movement toward the load's destination, the MPC cost function is defined based on the APF as follows:

$$J = \sum_{j=1}^{N+1} F_p(j) + \sum_{j=1}^{N+1} F_{ob}(j) + kT \tag{9}$$

where k is a positive constant, T and N are the runtime and the number of iterations of the algorithm, respectively. By choosing the cost function as in (9), the load is ensured to avoid obstacles and move toward the destination as quickly as possible when the optimal solution of J is found.

The physical constraints of the crane system during the MPC optimization process are established as follows:

$$\begin{aligned}
&l_{min} \le l(j) \le l_{max},\\
&\theta_{\min} \le \theta(j) \le \theta_{\max},\\
&0 \le \dot{x}(j) \le \dot{x}_{max},\\
&\dot{l}_{\min} \le \dot{l}(j) \le \dot{l}_{\max},\\
&\dot{\theta}_{\min} \le \dot{\theta}(j) \le \dot{\theta}_{\max},\\
&\ddot{x}_{\min} \le \ddot{x}(j) \le \ddot{x}_{\max},\\
&\ddot{l}_{\min} \le \ddot{l}(j) \le \ddot{l}_{\max},\\
&\ddot{\theta}_{\min} \le \ddot{\theta}(j) \le \ddot{\theta}_{\max},\\
&-g < \ddot{z}_l(j)\\
&0 < T \le T_{\max}
\end{aligned} \tag{10}$$

where $g < \ddot{z}_l(j)$ to prevent the hoisting cable from slackening, and the remaining states are constrained as in (10) to comply with practical operating conditions.

Remark 3. *When optimizing the cost function J and ensuring the crane's physical constraints through the MPC controller, the obtained solution satisfies the specified requirements, including obstacle avoidance, compliance with kinematic constraints, and motion time optimization. At the same time, with the reference signals for the trolley and hoisting cable determined, the load swing angle is also maintained within allowable limits. Therefore, in the trajectory tracking control phase, the anti-sway controller can be omitted; as evidence, the gain coefficients related to the swing angle are set to zero. The block diagram of the reference trajectory design method using MPC-APF is presented in detail in Figure 4.*

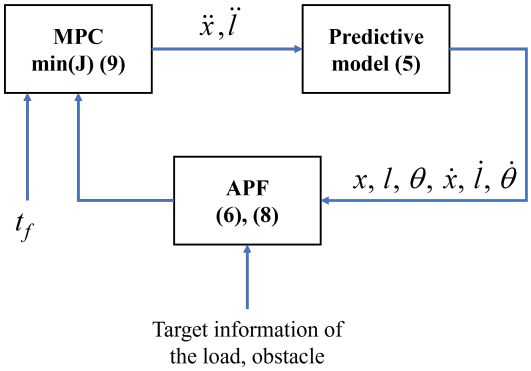

Figure 4: MPC-APF structure

3. Trajectory tracking control design

In this section, the SMC is designed to control the trolley to track the trajectory constructed in the previous section.

3.1 Sliding mode control

Let $\boldsymbol{X} = [x, l, \theta]^\top$ and $\boldsymbol{U} = [u_1, u_2]^\top$. From (1), the dynamics of the crane system can be rewritten as follows:

$$\boldsymbol{M}(\boldsymbol{X})\ddot{\boldsymbol{X}} + \boldsymbol{C}(\boldsymbol{X}, \dot{\boldsymbol{X}})\dot{\boldsymbol{X}} + \boldsymbol{G}(\boldsymbol{X}) = \boldsymbol{D}\boldsymbol{U} \tag{11}$$

where $\boldsymbol{M} = \begin{bmatrix} m_r + m & m\sin\theta & ml\cos\theta \\ m\sin\theta & m & 0 \\ ml\cos\theta & 0 & ml^2 \end{bmatrix}$, $\boldsymbol{G} = \begin{bmatrix} 0 \\ -mg\cos\theta \\ mgl\sin\theta \end{bmatrix}$, $\boldsymbol{C} = \begin{bmatrix} 0 & 2m\cos\theta\dot{\theta} & -ml\sin\theta\dot{\theta} \\ 0 & 0 & -ml\dot{\theta} \\ 0 & 2ml\dot{\theta} & 0 \end{bmatrix}$, and $\boldsymbol{D} = \begin{bmatrix} 1 & 0 \\ 0 & 1 \\ 0 & 0 \end{bmatrix}$.

The acceleration $\ddot{\boldsymbol{X}}$ is computed from (11) by using the inverse of the matrix $\boldsymbol{M}$:

$$\ddot{\boldsymbol{X}} = \boldsymbol{M}^{-1}\left(-\boldsymbol{C}\dot{\boldsymbol{X}} - \boldsymbol{G} + \boldsymbol{D}\boldsymbol{U}\right) \tag{12}$$

Given the reference trajectory $\boldsymbol{X}_d = [x_d, l_d, \theta_d]^\top$, the crane's trajectory tracking error is defined as follows:

$$\boldsymbol{e}_X = \boldsymbol{X} - \boldsymbol{X}_d \tag{13}$$

To ensure the convergence of the trajectory tracking error, the sliding surface is chosen as follows:

$$\boldsymbol{s} = \dot{\boldsymbol{e}}_X + \boldsymbol{c}\boldsymbol{e}_X \tag{14}$$

where $\boldsymbol{c} = \mathrm{diag}(c_x, c_l, 0)$, with c_x, c_l are positive constants.

The derivative of the sliding surface in (14) is determined as follows:

$$\begin{aligned}
\dot{\boldsymbol{s}} &= \ddot{\boldsymbol{e}}_X + \boldsymbol{c}\dot{\boldsymbol{e}}_X\\
&= \ddot{\boldsymbol{X}} - \ddot{\boldsymbol{X}}_d + \boldsymbol{c}\dot{\boldsymbol{e}}_X\\
&= \boldsymbol{M}^{-1}\left(-\boldsymbol{C}\dot{\boldsymbol{X}} - \boldsymbol{G} + \boldsymbol{D}\boldsymbol{U}\right) - \ddot{\boldsymbol{X}}_d + \boldsymbol{c}\dot{\boldsymbol{e}}_X
\end{aligned} \tag{15}$$

According to the constant rate reaching control law, the control input $\boldsymbol{U}$ is determined as follows:

$$\boldsymbol{U} = \left(\boldsymbol{D}^\top\boldsymbol{D}\right)^{-1}\boldsymbol{D}^\top\left(\boldsymbol{G} + \boldsymbol{C}\dot{\boldsymbol{X}} - \boldsymbol{M}\left(\boldsymbol{k}\,\mathrm{sign}(\boldsymbol{s}) - \ddot{\boldsymbol{X}}_d + \boldsymbol{c}\dot{\boldsymbol{e}}_X\right)\right) \tag{16}$$

where $\boldsymbol{k} = \mathrm{diag}(k_{s_x}, k_{s_l}, 0)$ with k_{s_x}, k_{s_l} are positive constants, and $\mathrm{sign}(\boldsymbol{s})$ is sign function.

3.2 Stability analysis

The stability of the crane system is stated in the following theorem.

Theorem 1. *If the system in (1) uses the controller in (16) with the sliding surface in (14), then the states $\boldsymbol{X}$ will converge to the reference trajectory $\boldsymbol{X}_d$.*

Proof. To prove stability, the Lyapunov function is chosen as $V = \frac{1}{2}\boldsymbol{s}^\top \boldsymbol{s}$. From (15) and (16), the derivative of the Lyapunov function is determined as follows:

$$\begin{aligned} \dot{V} &= -\boldsymbol{s}^\top \dot{\boldsymbol{s}} \\ &= -\boldsymbol{s}^\top \boldsymbol{k}\,\mathrm{sign}(\boldsymbol{s}) \\ &\le -\lambda_{\min}(\boldsymbol{k})\,\boldsymbol{s}^\top \boldsymbol{s} \le 0 \end{aligned} \tag{17}$$

In this case, the sliding surface will converge to zero rapidly, ensuring that the trajectory tracking errors converge to a neighborhood around zero.

Remark 4. *To mitigate high-frequency oscillations in the control signal, which are common in conventional sliding mode control, we use the function* $\tanh(\zeta \boldsymbol{s})$ *to replace the* $\mathrm{sign}(\boldsymbol{s})$ *function, as described below:*

$$\tanh(\zeta \boldsymbol{s}) = \frac{e^{\zeta \boldsymbol{s}} - e^{-\zeta \boldsymbol{s}}}{e^{\zeta \boldsymbol{s}} + e^{-\zeta \boldsymbol{s}}} \tag{18}$$

In this case, the control vector $\boldsymbol{U}$ becomes:

$$\boldsymbol{U} = \left(\boldsymbol{D}^\top \boldsymbol{D}\right)^{-1} \boldsymbol{D}^\top \left(\boldsymbol{G} + \boldsymbol{C}\dot{\boldsymbol{X}} - \boldsymbol{M}\left(\boldsymbol{k}\tanh(\zeta \boldsymbol{s}) - \ddot{\boldsymbol{X}}_d + \boldsymbol{c}\dot{\boldsymbol{e}}_X\right)\right) \tag{19}$$

4. Simulation verification

4.1 Simulation setting

In this section, we validate the proposed obstacle avoidance motion planning method using Matlab/Simulink. The crane model parameters are selected according to [12]: $m = 0.74$ kg, $m_r = 1.155$ kg, $g = 9.81$ m/s^2.

We implement a scenario in which the crane moves the load from position (0,-4) to (6,-3), with the load swing angle at both the starting and target points set to 0 degrees. The obstacle is a rectangle with vertices at (2.5,-5), (3,-5), (3,-2.5), and (2.5,-2.5), covered by three circles as illustrated in Figure 3. The design parameters of the MPC-APF are chosen as $A_p = 10, A_{ob} = 35, \sigma = 0.5$, and $k = 100$, while the parameters of the SMC are set as $\boldsymbol{c} = \mathrm{diag}(5,5,0)$ and $\boldsymbol{k} = \mathrm{diag}(10,10,0)$. The physical constraints of the crane during the trajectory optimization process are established as follows:

$$\begin{aligned} 0.5\,\mathrm{m} \le l(j) \le 6\,\mathrm{m}, \\ -\frac{\pi}{60}\,\mathrm{rad} \le \theta(j) \le \frac{\pi}{60}\,\mathrm{rad}, \\ 0 \le \dot{x}(j) \le 2\,\mathrm{m/s}, \\ -1\,\mathrm{m/s} \le \dot{l}(j) \le 1\,\mathrm{m/s}, \\ -0.3\,\mathrm{rad/s} \le \dot{\theta}(j) \le 0.3\,\mathrm{rad/s}, \\ -2\,\mathrm{m/s^2} \le \ddot{x}(j) \le 2\,\mathrm{m/s^2}, \\ -1\,\mathrm{m/s^2} \le \ddot{l}(j) \le 1\,\mathrm{m/s^2}, \\ -0.75\,\mathrm{rad/s^2} \le \ddot{\theta}(j) \le 0.75\,\mathrm{rad/s^2}, \\ -g < \ddot{z}_l(j) \\ 0 < T \le 10\,\mathrm{s} \end{aligned} \tag{20}$$

The simulation results are presented in the following section.

4.2 Simulation results

In this section, we sequentially present the motion trajectory optimization results based on MPC-APF and the trajectory tracking control results using SMC.

4.2.1 Results of motion planning

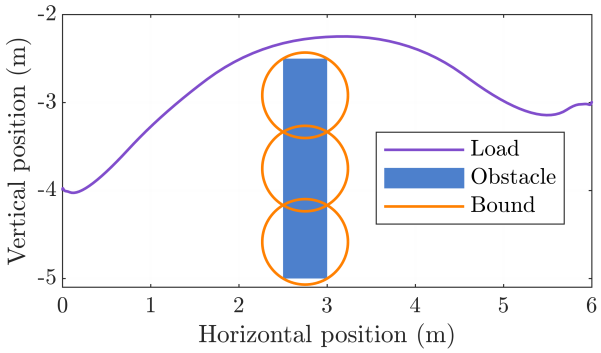

Figure 5: Optimal trajectory of the load during obstacle avoidance

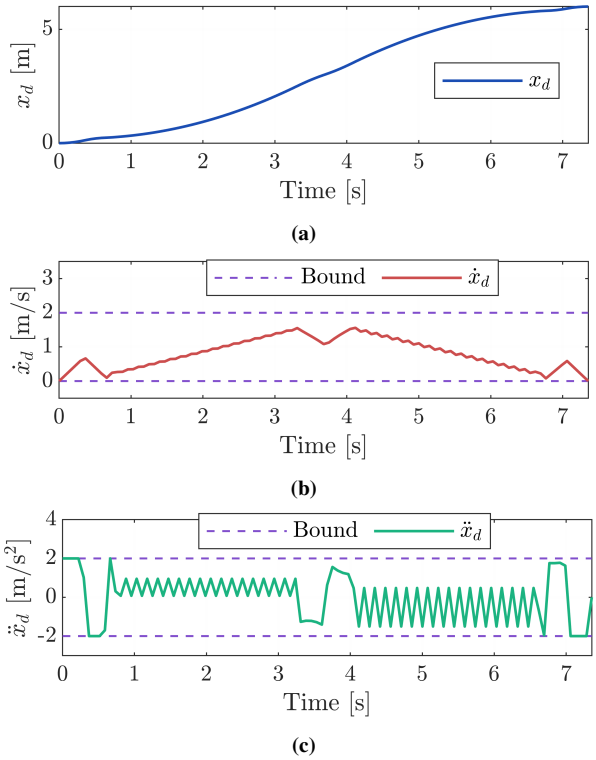

Figure 6: Optimal horizontal trajectory: (a) Position, (b) velocity, (c) acceleration

The reference lateral position of the trolley after optimization by MPC-APF is shown in Figure 6. In particular, Figures 6b and 6c illustrate that the reference lateral velocity and acceleration fully comply with the constraints established in the MPC design. Similar results are also observed for the variation of the hoisting cable length, as described in Figure 7. The responses related to the load motion are presented in Figure 8. It can be observed that with x_d and l_d in Figures 6 and 7, the

physical constraints including the amplitude, angular velocity, and angular acceleration of θ_d are all satisfied.

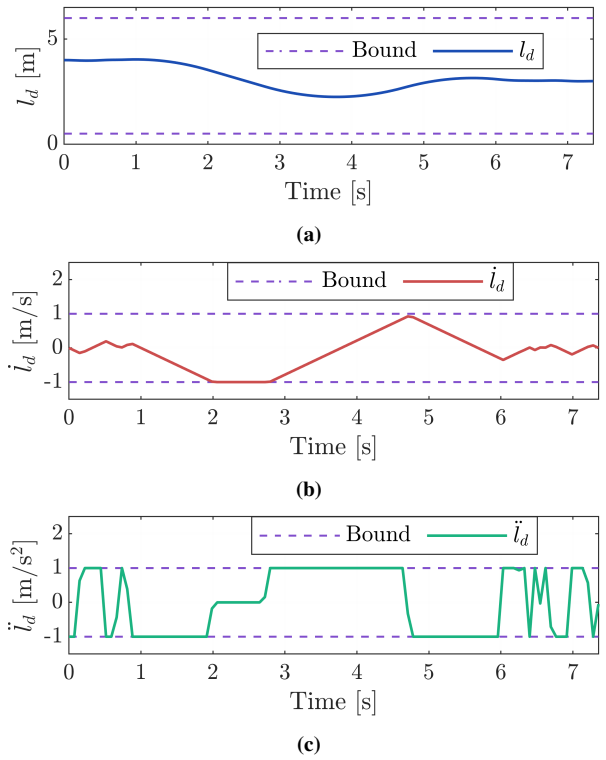

Figure 7: Hoisting cable: (a) Length, (b) rate of change, (c) acceleration of change

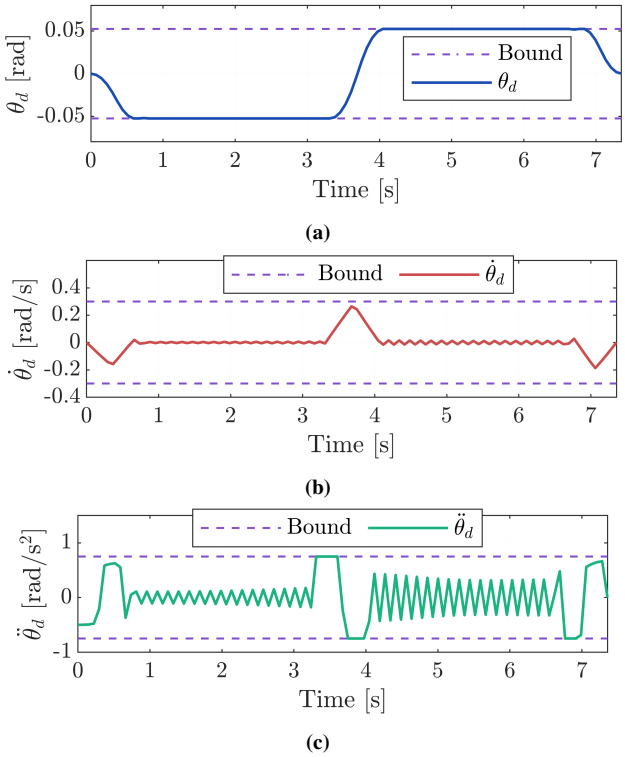

Figure 8: Load swing angle: (a) Amplitude, (b) angular velocity, (c) angular acceleration

The trajectory of the load corresponding to the above reference states is illustrated in Figure 5. It can be seen that the obtained trajectory is smooth and completely free of collisions with the obstacle. At the same time, the travel time for the load to reach the destination, as observed in Figures 6–8, is about 7 seconds, shorter than the 10 seconds in the initial setup. This result demonstrates that MPC successfully determined the optimal motion trajectory, balancing three factors: obstacle avoidance, reaching the destination, and reducing travel time. In this simulation, MPC performs 180 iterations to find the optimal trajectory, with the value of the cost function J at each iteration shown in Figure 9. It can be seen that after approximately 170 iterations, MPC converges to the optimal solution and provides the result at the 180th iteration.

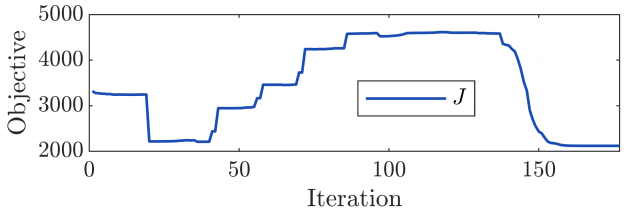

Figure 9: Cost function variation with the number of iterations

4.2.2 Results of trajectory tracking

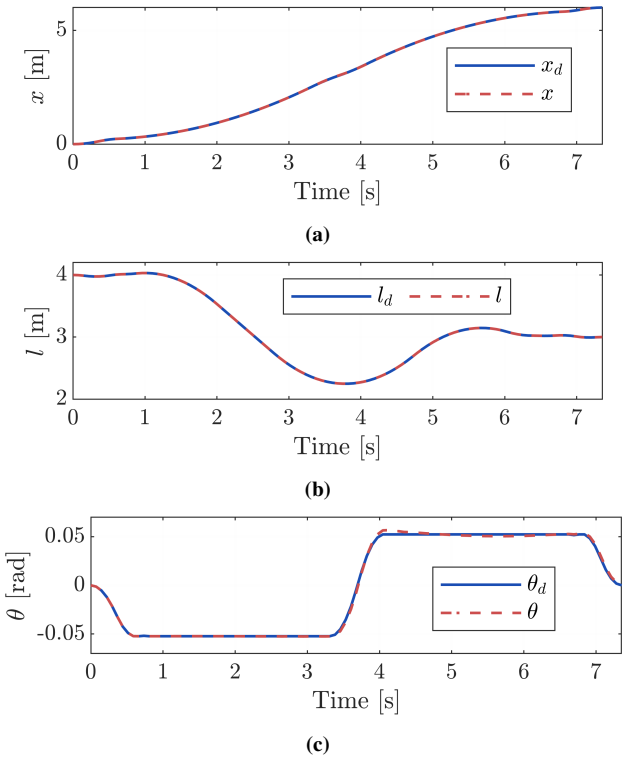

Figure 10: Trajectory tracking response: (a) Horizontal position of the trolley, (b) hoisting cable length, (c) load swing angle

After determining the obstacle-avoidance trajectory of the crane based on MPC-APF, the traction force acting on the trolley and the hoisting/lowering force of the suspension cable are computed by the SMC to control the crane in tracking the reference trajectory. The crane states, including the lateral position, suspension cable length, and load swing angle, are presented in Figure 10. The results show that these states closely follow their corresponding reference values, with the tracking errors

shown in Figures 11a, 11b, and 11c, respectively. A closer look at Figure 11 reveals that the tracking error of the load swing angle is significantly larger than the other two errors. The reason is that variations in the load swing angle depend entirely on the motion of the trolley and the suspension cable, which leads to a tendency for the swing angle tracking error to be greater. The traction force acting on the trolley and the hoisting/lowering force of the suspension cable are presented in Figure 12.

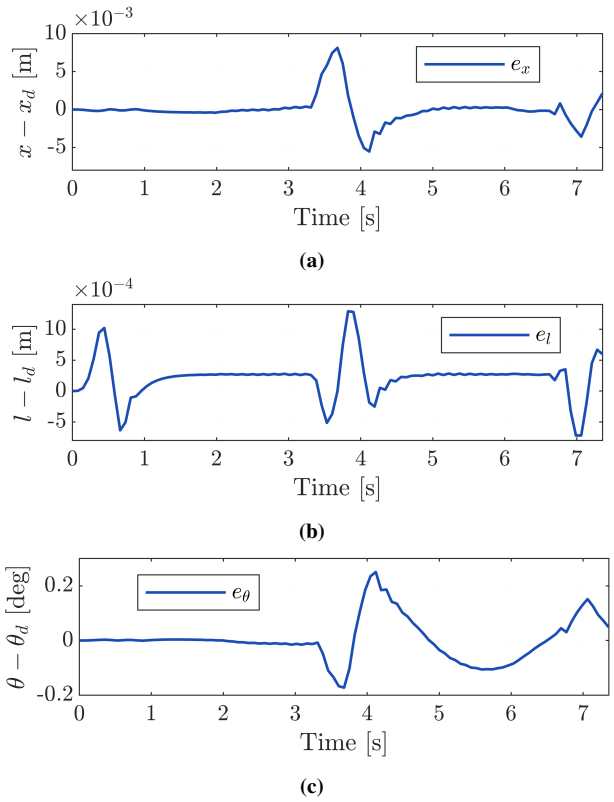

Figure 11: Trajectory tracking error: (a) Trolley horizontal position, (b) hoisting cable length, (c) load swing angle

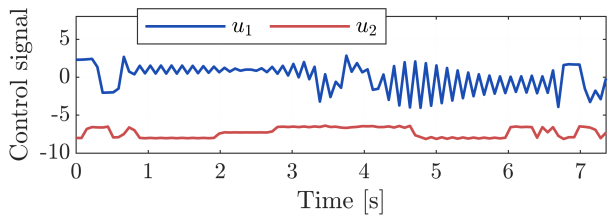

Figure 12: Control signal: (a) Driving force applied to the trolley, (b) force for hoisting/lowering the load cable.

4.3 Discussion

From the above simulation results, the feasibility of MPC-APF in obstacle avoidance applications for cranes can be confirmed. The design of the artificial potential field, consisting of attractive and repulsive potentials, enables the construction of the cost function J. Subsequently, optimizing J using MPC expands the feasible solution set thanks to its soft-constraint characteristics, thereby overcoming the limitations of existing methods that rely on hard constraints.

A limitation of the proposed obstacle avoidance algorithm is the occurrence of slight chattering in the states and control signals. The reason is that (5) models the dynamic relationship between the swing angle and the trolley position as well as the suspension cable length only in the form of first-order derivatives, where the input $\boldsymbol{u}$ corresponds to the acceleration of the trolley position and cable length. To mitigate chattering in the responses, higher-order derivatives (third-order or above) of x and l can be used in the input $\boldsymbol{u}$, thereby smoothing the optimal trajectory when passing through the integration stages.

5. Conclusion

This paper has proposed a novel obstacle avoidance motion planning strategy for crane systems, in which the optimal trajectory is determined by optimizing the cost function through MPC. The cost function is designed to account for three factors: the attractive potential field, the repulsive potential field, and the travel time of the load to the destination. The simulation results have demonstrated the advantages of the proposed method, particularly the integration of MPC and APF, which enables the crane to both avoid obstacles and satisfy physical constraints. In the future, we will extend this strategy to crane systems in 3D environments and integrate it with a trajectory tracking control system.

6. Acknowledgment

This research was funded by the Vietnam National Foundation for Science and Technology Development (NAFOSTED).

References

[1] M. N. Vu, A Lobe, F. Beck, T. Weingartshofer, C. Hartl-Nesic, and A. Kugi, "Fast trajectory planning and control of a lab-scale 3d gantry crane for a moving target in an environment with obstacles," *Control Engineering Practice*, vol. 126, p. 105 255, 2022.

[2] H. L. Thi, T. L. Nguyen, et al., "Adaptive finite-time extended state observer-based model predictive control with flatness motivated trajectory planning for 5-dof tower cranes," *European Journal of Control*, vol. 81, p. 101 149, 2025.

[3] B. Fan, Y. Zhao, H. Zhou, J. Wang, and L. Sun, "Load energy coupling-based underactuated control method on trajectory planning and antiswing for bridge cranes," *Journal of Computational and Nonlinear Dynamics*, vol. 20, no. 5, p. 051 001, 2025.

[4] W. Tang, R. Ma, W. Wang, and H. Gao, "Optimization-based input-shaping swing control of overhead cranes," *Applied Sciences*, vol. 13, no. 17, p. 9637, 2023.

[5] F. M. Barbosa, A. Kullberg, and J. Löfberg, "Fast or cheap: Time and energy optimal control of ship-to-shore cranes," *IFAC-PapersOnLine*, vol. 56, no. 2, pp. 3126–3131, 2023.

[6] D. Jolevski, O. Bego, and D. Jakus, "Modified smith input-shaper crane-controller for position control and sway reduction," *Applied Sciences*, vol. 15, no. 5, p. 2804, 2025.

[7] H. B. T. Khanh, M. H. Thi, L. T. Hue, T. L. Nguyen, and D. H. Nguyen, "Flatness-based motion planning and model predictive control of industrial cranes," *Engineering, Technology & Applied Science Research*, vol. 14, no. 4, pp. 15 141–15 148, 2024.

[8] T. Kusznir and J. Smoczek, "Nonlinear model predictive control with evolutionary data-driven prediction model and particle swarm optimization optimizer for an overhead crane," *Applied Sciences*, vol. 14, no. 12, p. 5112, 2024.

[9] S. Iftikhar, O. J. Faqir, and E. C. Kemgan, "Nonlinear model predictive control of an overhead laboratory-scale gantry crane with obstacle avoidance," in *2019 IEEE Conference on Control Technology and Applications (CCTA)*, IEEE, 2019, pp. 382–387.

[10] H. Chen, Y. Fang, and N. Sun, "A time-optimal trajectory planning strategy for double pendulum cranes with swing suppression," in *2016 35th Chinese Control Conference (CCC)*, IEEE, 2016, pp. 4599–4604.

[11] G. Li, X. Ma, Z. Li, and Y. Li, "Time-polynomial-based optimal trajectory planning for double-pendulum tower crane with full-state constraints and obstacle avoidance," *IEEE/ASME Transactions on Mechatronics*, vol. 28, no. 2, pp. 919–932, 2022.

[12] L. Ramli, Z Mohamed, M. Efe, I. M. Lazim, and H. Jaafar, "Efficient swing control of an overhead crane with simultaneous payload hoisting and external disturbances," *Mechanical systems and signal processing*, vol. 135, p. 106 326, 2020.

[13] H. Luu Thi and T. L. Nguyen, "A novel non-recursive control for payload positioning and swing suppressing problems in overhead-crane applications," *Transactions of the Institute of Measurement and Control*, p. 01 423 312 251 344 994, 2025.

[14] J.-F. Duhé, S. Victor, and P. Melchior, "Contributions on artificial potential field method for effective obstacle avoidance," *Fractional Calculus and Applied Analysis*, vol. 24, no. 2, pp. 421–446, 2021.